Theoretical Investigation for MESP, HOMO-LUMO and FTIR analysis of N-Chlorophenyl Based Acetamide

Zunnaira Hakeem[1], Hina Masood[2], Saba Nosheen[1], Muhammd Imran[1], Narmeen Ali[2], Laiba Waris[1], Majid Ali[1*], Zahra Hanif[1], Sidra Ghafoor[2], Samiuddin[1]

[1]Department of Chemistry, Faculty of Engineering and Applied Sciences, Riphah International University Faisalabad, Pakistan
[2]Department of Chemistry, Government College University Faisalabad, Pakistan

Abstract

In presented work, the density functional theory (DFT) was employed to check the molecular behavior of N-chlorophenyl based acetamide compound in variety of solvents. Properties such as vibrational frequency, energetic parameters and MESP properties of N-chlorophenyl based acetamide were found, moreover their dihedral angle, including bond length were also studied to find the geometry of the molecule. The findings of the FTIR spectra indicated that their peaks have precise vibrational assignments. The wavenumbers of the majority of the modes fell within the expected range of the transmittance. This study has been conducted on the electrostatic potential of the molecule to predict relative reactivates and electrophilic and nucleophilic sites. In order to calculate the atomic charges, electronic exchange interactions, changes in the molecule's energy with charge delocalization, HOMO & LUMO studies were defined. The molecular electronic potential (MEP) of the molecule was obtained in solid, mesh, and transparent forms to investigate global and local reactivity characteristics. The theoretical study was carried out to provide complete understanding of the molecule for future applications.

Keywords: UV analysis, MEP, HOMO-LUMO, vibrational study, density functional theory

1. INTRODUCTION

N-chlorophenyl based acetamides

Acetamide-N-phenyl compounds are essential ingredients in medicines, stabilizers, and colors. It is challenging to produce amines directly from carboxylic acids because an acidic carboxyl group is converted into its carboxylate anion by the base found in amines (Ammar et al., 2021). As a result, the carboxylic acid is changed into an acylating agent called an acyl halide, which interacts with the amine quickly. Carboxylic acid can be converted into an

acyl halide in a number of methods, including by utilizing phosphorous pentachloride and thionyl chloride on substances that don't have functional groups that are acid-sensitive.

. These class compounds use as antibiotic resistance has emerged as one of the most significant global public health concerns in the last 10 years as a result of antibiotic abuse. Therefore, developing new antibacterial drugs requires overcoming multidrug resistance (MDR). The pharmacological and biological properties of the N-phenylacetamide derivatives, which include anti-bacterial, anticonvulsant, antimicrobial, and HIV-1 inhibitor, are widely recognized. A number of authorized medications, including the antiviral Inosine Pranobex, the beta-adrenergic antagonist Practolol, and the local anesthetic Etidocaine, contain N-phenylacetamine as a structural component (B et al., 2021).

Derivatives of quinolones have been successfully used for many years to treat parasitic illnesses that are transmitted by mosquitos. Several medications in this class have been studied for their antiviral, bactericidal, antimicrobial, anti-inflammatory, and antiprotozoal properties. Consequently, several compounds of anilidoquinoline were synthesized and their antiviral efficacy were evaluated. It has been demonstrated that 2-(2-methyl-quinoline-4ylamino)-N-(2-chlorophenyl)-acetamide (PP2) is a useful agent for JEV protection. (Bagayoko, 2014). 2,4-diamino-6-hydroxy-5-nitroso pyrimidine, 2-mercapto pyrimidine, pyrazinamide, and molecular and spectral analysis supported by DFT Deuterium-substituted fluocytosine, 4-aminopyrimidine, 2-amino-5-nitropyrimidines, and Quantum calculations have been performed on all 4-aminopyrimidines, and the vibrational bands have been published. For sulfanyl-aminobenzene, stretching frequencies have been determined. The type of substituent at the pyrimidine ring's 2- and 6-positions has been demonstrated to have a significant influence on the anti-tubercular action. The structural analysis of chloropyrimidine-based antimicrobial compounds is also found in literature. These compounds work against *M. tuberculosis (Erdem Büyükkiraz & Kesmen, 2022)*. The molecule in the work has garnered attention due to its structure, biological activity spectrum, and functional group. In contrast, there hasn't been done any study yet for this selected acetamide compound using DFT. As part of combination antiretroviral therapy, Ritonavir, Darunavir, and Lamivudine/Zidovudine were initiated; nevertheless, they had no effect on the

cerebellar dysfunctions associated with HIV infection, such as ataxia, dementia, and neurocognitive deficits (Zaman et al., 2023).

In current work, 2-((5-((2-chlorophenyl)(6,7-dihydrothieno[3,2-c]pyridin-5(4H)-yl)methyl)-1,3,4-oxadiazol-2-yl)thio)-N-(p-tolyl) acetamide compound was investigated with DFT/6-31/B3LYP model.

2. Materials

2.1 Chemicals

Acetone, ethanol, water, and other solvents were used in this investigation to investigated the compound affinities. The compound under investigation has IUPAC name, 2-((5-((2-chlorophenyl)(6,7-dihydrothieno[3,2-c]pyridin-5(4H)-yl)methyl)-1,3,4-oxadiazol-2-yl)thio)-N-(p-tolyl) acetamide (CPA).

Figure (b)

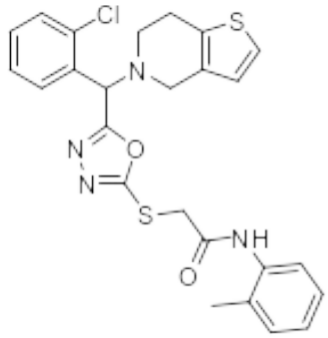

Figure (2a)

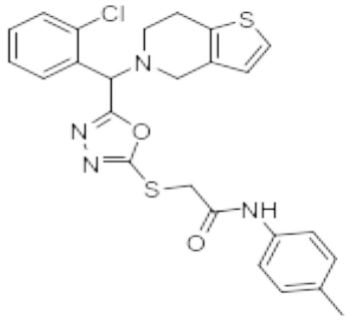

Figure (2b)

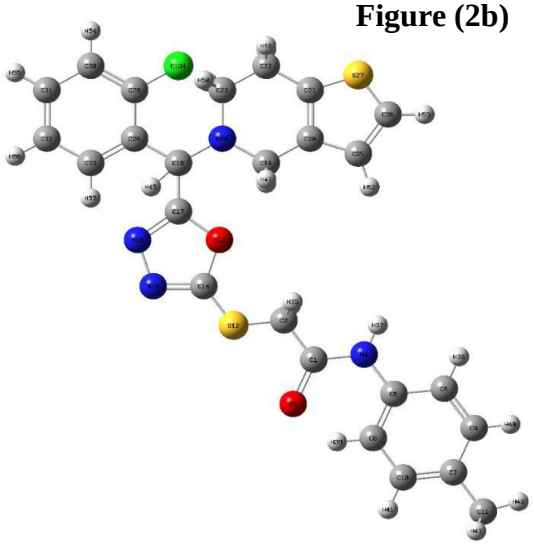

Figure 2.1: Optimized Structure of CPA

2.2 Methodology

The computations were done using Gaussian 09 software. 6-311G++ basis set with B3LYP correction using the DFT technique was applied to improve the geometries in Gaussian 09 analytical gradients. The CPA geometry have been established using the same theoretical levels (Baboul, Curtiss, Redfern, & Raghavachari, 1999). The absorption spectra of the molecule have been obtained in gas, water, and a few other solvents with same model used for geometry calculation. The potential energy hypersurface minima's stationary nature was confirmed without any imaginary frequency. Furthermore, Moltran software was used to compute the thermodynamic properties of the CPA. For, vibrational assessment the VEDA 4 program was employed. GaussView 05 and chem 3D were used for drawing structure. Origin pro was employed for graphical purpose.

3 RESULTS AND DISCUSSION

3.1 Geometry Calculations

It is often known that precisely identifying the basic characteristics of compounds can be difficult. However, using quantum mechanical calculations is an efficient way to deal with this problem. DFT was utilized in this work to calculate the structural geometry of CPA with 6-31G(d) basis set and the B3LYP functional. The computations were carried out in different solvents and in the gas phase. Following a comparison with experimental data, the acquired results showed a high degree of agreement between the calculated and observed values in Table 3.1 (Siddiqua et al., 2020).

Table 3.1: Bond lengths of CPA in gas and different solvents

Computed Bond lengths				MP2				
Parameter	**Gas**	**Water**	**Ethanol**	**Acetone**	**Gas**	**Water**	**Ethanol**	**Acetone**
C22,C20	1.4397	1.4397	1.4397	1.4397	1.4397	1.4397	1.4397	1.4397
C20,C21	1.4888	1.4888	1.4888	1.4888	1.4888	1.4888	1.4888	1.4888
C22,S25	1.7099	1.7099	1.7099	1.7099	1.7099	1.7099	1.7099	1.7099
C21,C22	1.4998	1.4998	1.4998	1.4998	1.4998	1.4998	1.4998	1.4998
C22,H25	1.0902	1.0902	1.0902	1.0902	1.0902	1.0902	1.0902	1.0902
C25,H48	1.0998	1.0998	1.0998	1.0998	1.0998	1.0998	1.0998	1.0998
C24,N49	1.3889	1.3889	1.3889	1.3889	1.3889	1.3889	1.3889	1.3889
C22,H51	1.0911	1.0911	1.0911	1.0911	1.0911	1.0911	1.0911	1.0911
C2,-H52	1.0789	1.0789	1.0789	1.0789	1.0789	1.0789	1.0789	1.0789
C22,C25	1.2229	1.2229	1.2229	1.2229	1.2229	1.2229	1.2229	1.2229
C23,H51	1.0607	1.0607	1.0607	1.0607	1.0607	1.0607	1.0607	1.0607
C25,S26	1.7092	1.7092	1.7092	1.7092	1.7092	1.7092	1.7092	1.7092
C27,H52	1.0753	1.0753	1.0753	1.0753	1.0753	1.0753	1.0753	1.0753
C27,C28	1.2897	1.2897	1.2897	1.2897	1.2897	1.2897	1.2897	1.2897
C27,C30	1.2997	1.2997	1.2997	1.2997	1.2997	1.2997	1.2997	1.2997
C28,C33	1.2899	1.2899	1.2899	1.2899	1.2899	1.2899	1.2899	1.2899
C27,C30	1.7867	1.7867	1.7867	1.7867	1.7867	1.7867	1.7867	1.7867
C33,C34	1.2986	1.2986	1.2986	1.2986	1.2986	1.2986	1.2986	1.2986
C31,H52	1.0789	1.0789	1.0789	1.0789	1.0789	1.0789	1.0789	1.0789
C32,C33	1.4908	1.4908	1.4908	1.4908	1.4908	1.4908	1.4908	1.4908
C32,H54	1.069	1.069	1.069	1.069	1.069	1.069	1.069	1.069
C31,C32	1.299	1.299	1.299	1.299	1.299	1.299	1.299	1.299
C33,H54	1.0877	1.0877	1.0877	1.0877	1.0877	1.0877	1.0877	1.0877
C32,H56	1.0789	1.0789	1.0789	1.0789	1.0789	1.0789	1.0789	1.0789

Table 3.2: Bond angles of CPA

Bond angles *(A* °)								
	Computed bond angles				**Experimental bond angles with MP2 method**			
Parameters	**Gas**	**Water**	**Ethanol**	**Acetone**	**Gas**	**Water**	**Ethanol**	**Acetone**
C1-N4-C5	127.8309	127.8309	127.8309	127.8309	127.8309	127.8309	127.8309	127.8309
C1-N4-H37	116.9147	116.9147	116.9147	116.9147	116.9147	116.9147	116.9147	116.9147
C5-N4-H37	115.2465	115.2465	115.2465	115.2465	115.2465	115.2465	115.2465	115.2465
N4-C5-C6	117.6999	117.6999	117.6999	117.6999	117.6999	117.6999	117.6999	117.6999
N4-C5-C8	123.3979	123.3979	123.3979	123.3979	123.3979	123.3979	123.3979	123.3979

S12-C14-O13	118.7567	118.7567	118.7567	118.7567	118.7567	118.7567	118.7567	118.7567
S12-C14-N15	128.8406	128.8406	128.8406	128.8406	128.8406	128.8406	128.8406	128.8406
O13-C14-N15	112.3978	112.3978	112.3978	112.3978	112.3978	112.3978	112.3978	112.3978
C14-N15-N16	105.9062	105.9062	105.9062	105.9062	105.9062	105.9062	105.9062	105.9062
N15-N16-C17	106.4364	106.4364	106.4364	106.4364	106.4364	106.4364	106.4364	106.4364
O13-C17-N16	111.8344	111.8344	111.8344	111.8344	111.8344	111.8344	111.8344	111.8344
O13-C17-C18	115.5977	115.5977	115.5977	115.5977	115.5977	115.5977	115.5977	115.5977
N16-C17-C18	132.5258	132.5258	132.5258	132.5258	132.5258	132.5258	132.5258	132.5258
C17-C18-N24	113.3581	113.3581	113.3581	113.3581	113.3581	113.3581	113.3581	113.3581
C17-C18-C28	111.2927	111.2927	111.2927	111.2927	111.2927	111.2927	111.2927	111.2927
C17-C18-H45	104.0032	104.0032	104.0032	104.0032	104.0032	104.0032	104.0032	104.0032
N24-C18-C28	112.8755	112.8755	112.8755	112.8755	112.8755	112.8755	112.8755	112.8755

Table 3.3: The dihedral angles of CPA

Dihedral angles (°)								
	Computed dihedral angles				Experimental dihedral angles with MP2 method			
Parameters	**Gas**	**Water**	**Ethanol**	**Acetone**	**Gas**	**Water**	**Ethanol**	**Acetone**
C22,C24,H45	113.1513	113.1513	113.1513	113.1513	113.1513	113.1513	113.1513	113.151
C25.C26,H54	111.5903	111.5903	111.5903	111.5903	111.5903	111.5903	111.5903	111.5903
C25,C26,S27	122.1499	122.1499	122.1499	122.1499	122.1499	122.1499	122.1499	122.1499
C22,C23,H52	111.2989	111.2989	111.2989	111.2989	111.2989	111.2989	111.2989	111.2989
C26,C24,H45	127.3278	127.3178	127.3178	127.3178	127.3178	127.3178	127.3178	127.3178
C22,S27,C24	120.3333	120.3333	120.3333	120.3333	120.3333	120.3333	120.3333	120.3333
C21,C26,C27	87.1198	87.1198	87.1198	87.1198	87.1198	87.1198	87.1198	87.1198
C18,C28,C33	123.9859	123.9859	123.9859	123.9859	123.9859	123.9859	123.9859	123.9859
C29,C28,C33	116.8999	116.8999	116.8999	116.8999	116.8999	116.8999	116.8999	116.8999
C29,C26,C33	118.0889	118.0889	118.0889	118.0889	118.0889	118.0889	118.0889	118.0889
C29,C28,C31	121.9209	121.9209	121.9209	121.9209	121.9209	121.9209	121.9209	121.9209
C29,C26,C33	122.1843	122.1843	122.1843	122.1843	122.1843	122.1843	122.1843	122.1843
C29-C30-C31	116.9998	116.9998	116.9998	116.9998	116.9998	116.9998	116.9998	116.9998
C28,C31,H52	118.6998	118.6998	118.6998	118.6998	118.6998	118.6998	118.6998	118.6998
C29,C31,H55	120.8403	120.8403	120.8403	120.8403	120.8403	120.8403	120.8403	120.8403
C29,C30,C31	119.8901	119.8901	119.8901	119.8901	119.8901	119.8901	119.8901	119.8901
C28,C31,H54	119.4999	119.4999	119.4999	119.4999	119.4999	119.4999	119.4999	119.4999
C29,C30,H54	119.7008	119.7008	119.7008	119.7008	119.7008	119.7008	119.7008	119.7008
C32,C33,C34	120.5998	120.5998	120.5998	120.5998	120.5998	120.5998	120.5998	120.5998
C32,C33,H54	119.5798	119.5798	119.5798	119.5798	119.5798	119.5798	119.5798	119.5798
C32,C31,H54	120.3998	120.3998	120.3998	120.3998	120.3998	120.3998	120.3998	120.3998
C29,C32,C33	119.8994	119.8994	119.8994	119.4994	119.8994	119.8994	119.8994	119.8994
C29,C32,H57	121.6979	121.6979	121.6979	121.6979	121.6979	121.6979	121.6979	121.6979
C32,C33,H57	118.9189	118.9189	118.9189	118.9189	118.9189	118.9189	118.9189	118.9189
N24,C18,H45,C17	119.2689	119.2689	119.2689	119.2689	119.2689	119.2689	119.2689	119.2689
N24,C18,H45,C17	-4.1169	-4.1169	-4.1169	-4.1169	-4.1169	-4.1169	-4.1169	-4.1169

3.2 Mulliken Charges Analysis

Applying quantum theory computations at the molecular level requires the computation of Mulliken atomic charges. It offers important details regarding the polarization, chemical reactions, and molecular structure of many substances. These charges were computed in different media. Table 3.4 shows negative values for N and O while for H values are positive showing their positivity/negativity worth. These findings advance our knowledge of the material's characteristics (Ansbacher et al., 2012).

Table 3.4: Mullikan Charge Values

Atom	Gas	Water	Ethanol	Acetone
C1	0.553345	0.553345	0.553345	0.553345
C 2	-0.611002	-0.611002	-0.611002	-0.611002
O3	-0.421149	-0.421149	-0.421149	-0.421149
N 4	-0.769089	-0.769089	-0.769089	-0.769089
C 5	0.312900	0.312900	0.312900	0.312900
C 6	-0.172989	-0.172989	-0.172989	-0.172989
C 7	0.126989	0.126989	0.126989	0.126989
C 8	-0.097888	-0.097888	-0.097888	-0.097888
C 9	-0.166916	-0.166916	-0.166916	-0.166916
C 10	-0.182686	-0.182686	-0.182686	-0.182686
C 11	-0.475441	-0.4765441	-0.475441	-0.475441
S 12	0.488779	0.488779	0.488779	0.488779
O 13	-0.478088	-0.478088	-0.478088	-0.478088
C 14	0.142948	0.142948	0.142948	0.142948
N 15	-0.294979	-0.294979	-0.294979	-0.294979
N 16	-0.243433	-0.243433	-0.243433	-0.243433
C 17	0.353978	0.353978	0.353978	0.353978
C 18	-0.07898	-0.07898	-0.07898	-0.07898
C 19	-0.150289	-0.150289	-0.150289	-0.150289
C 20	0.163989	0.163989	0.163989	0.163989

3.3 IR Study

The FTIR peaks indicate that acetone has displayed sharp peaks, and ethanol will likewise display lines with varying values (1679–2479) (Klähn et al., 2004). Gas and water will likewise display the transmittance that the graph peaks indicate. The transmittance values displayed in the graph below (Rani, Sundaraganesan, Kurt, Cinar, & Karabacak, 2010).

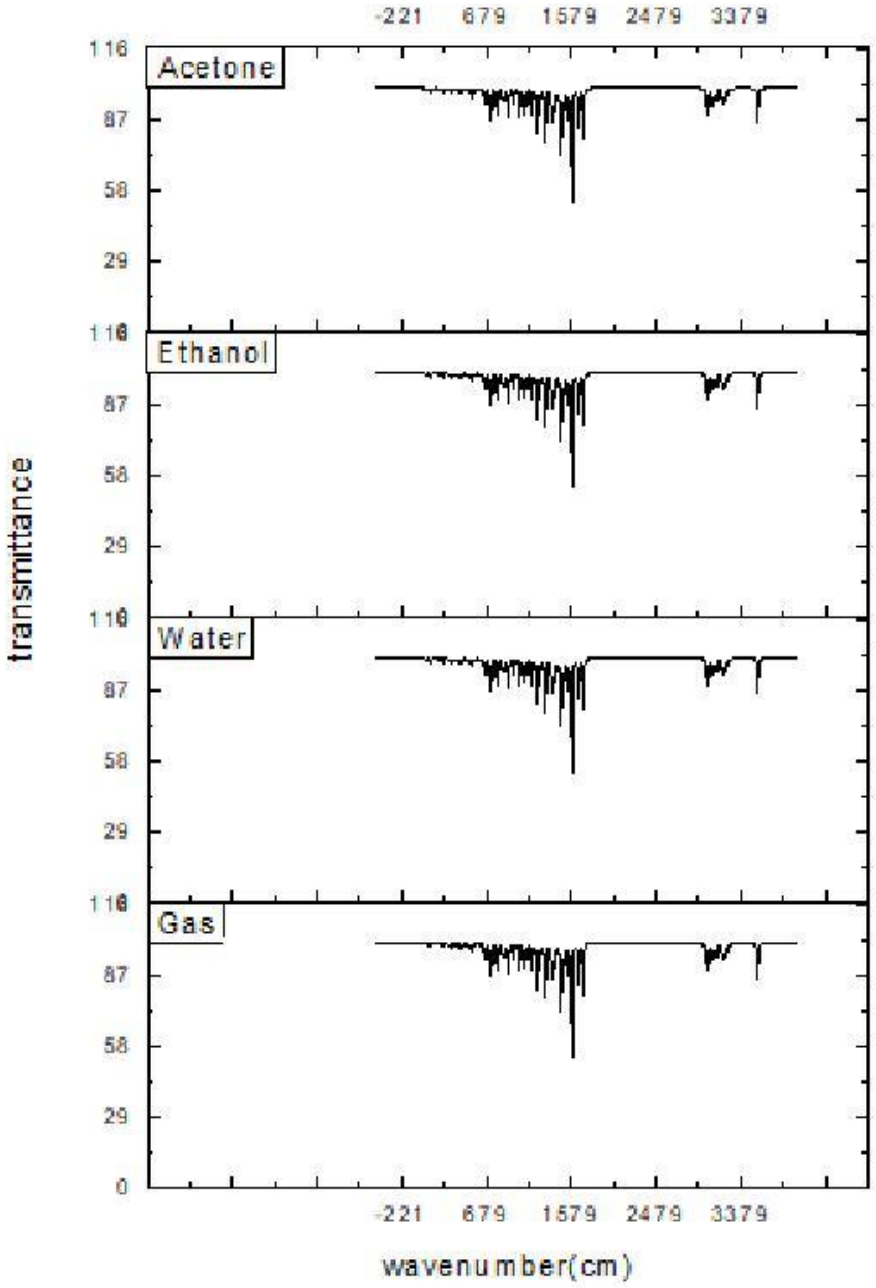

Figure 3.1: *IR Spectra of CPA*

3.4 Energy of HOMO-LUMO

Figure 3.2 displays the computed HOMO and L UMO orbitals at the B3LYP/6-31G level and it shows that their energy gaps were found to be the lowest-energy transitions.

To supply excitation energy, the formula

$$\Delta E = E_{HOMO} - E_{LUMO}$$

was used to compute the energy difference betw een the lowest unoccupied molecular orbital (L UMO) and the highest occupied molecular orbit al (HOMO) (Mumit et al., 2020).

These orbitals, HOMO and LUMO, are significant in any reaction.

The LUMO orbital can function as an acceptor of electrons, whereas the H OMO orbital is an electron donor.

The molecule's chemical stability and reactivity are disclosed by its energy gap.

Reduced stability and significant reactivity are indicated by the smaller energy difference betw een the orbitals (Zhang & Musgrave, 2007)

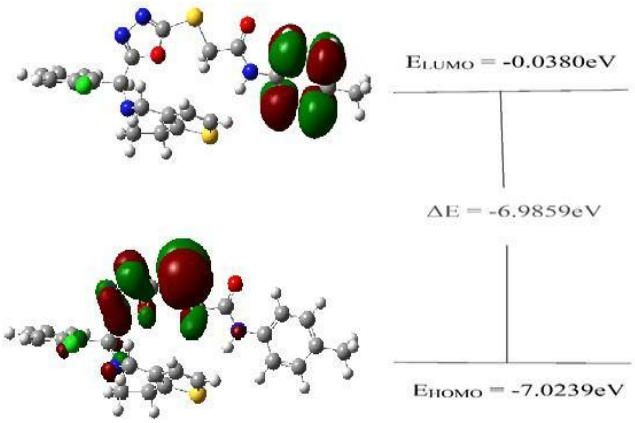

Figure 3.2:H-L energy gap of CPA in ethanol

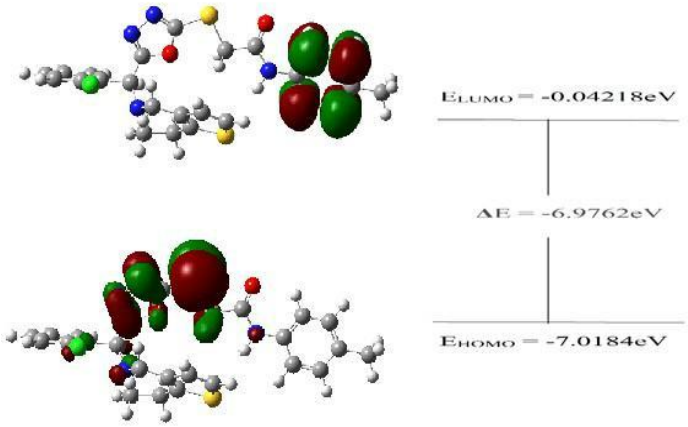

Figure 3.3: HOMO-LUMO energy gap of CPA in gaseous media

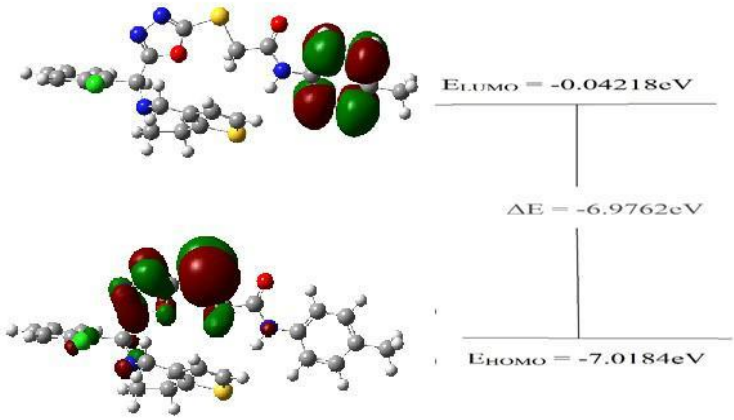

Figure 3.4: Energy gap of CPA in water

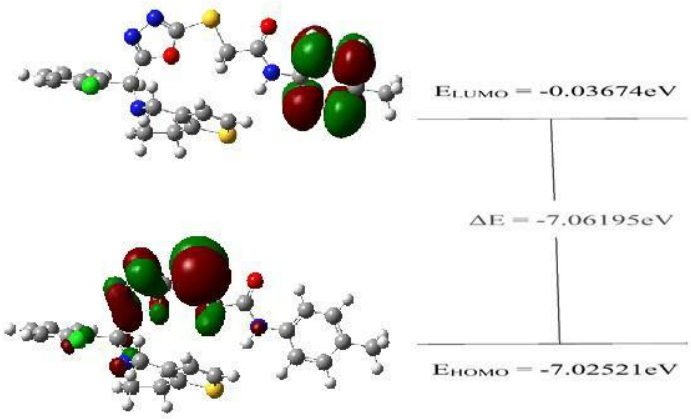

Figure 3.5: HOMO-LUMO energy gap of CPA in acetone

3.5 Molecular Electrostatic Potential (MEP)

The purpose of this analysis is to calculate the electron density distribution across the molecule electropositive and electronegative character. It is very useful in predicting how reactive a molecule will be to attacks from nucleophiles and electrophiles (Ali et al., 2018; Ali, Subhani, Farhat Ibraheem, Hafeez, & Sana). Additionally, it speculates on the kinds of intermolecular interactions that might occur. When an electrophilic assault occurs within a molecule, it will ideally target the most negatively charged area, or the region where the electron effect is most dominant. The MESP map of CPA produced on the isodensity surface is displayed in Figure 3.6. The area with blue colour is electropositive and has less electron density, whereas the red component represents negative charge and a higher electron density.

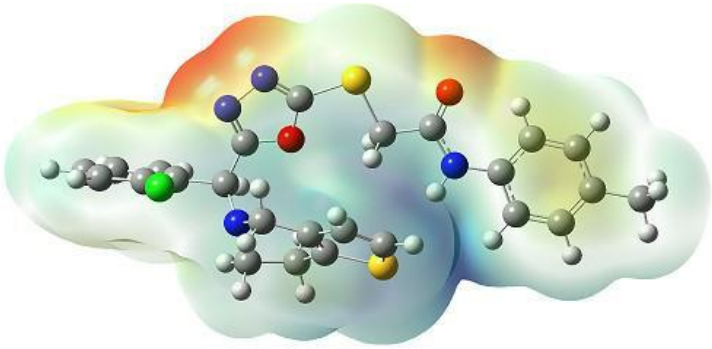

Figure 3.6: *MEP map for CPA*

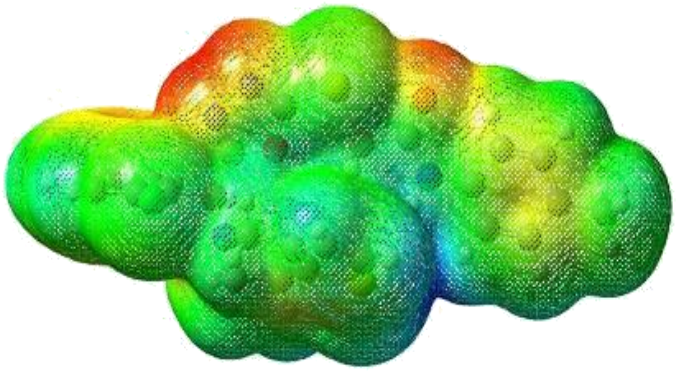

Figure 3.7: *mesh form*

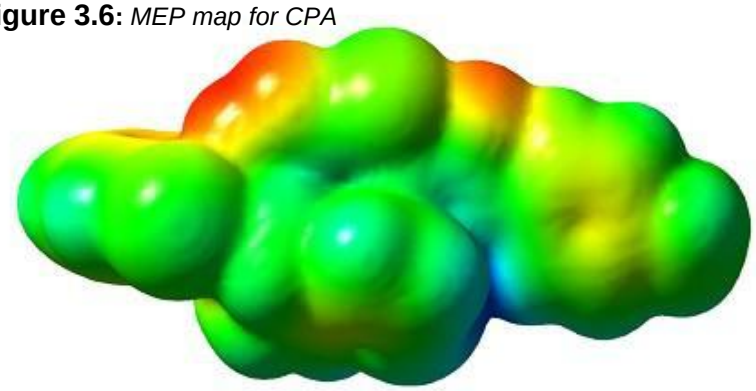

Figure 3.8: *solid mesh*

3.6 CONCLUSION

The computational work for CPA provided detailed information. Initially, we choose a set of tools for these computations. Guassview 6.0 and Guassion 09, tools that were used to calculate these compounds at various stages. The geometry, frequency, and energy of CPA molecule have been calculated. Following the output file calculations, FTIR and UV-Visible spectra with origin was obtained. The bond angle, bond length, and dihedral angles using several solvents, including ethanol, gas, acetone, and water were found. The same computations were done in DFT using function 6-311G and B3LYP. For NBO Analysis. Vibration analysis assisted in determining the vibrational modes of compound. The HOMO-LUMO energy gap in various solvents was found which aids in energy calculation. Additionally, the molecular electrical potential (MEP) was calculated in transparent, solid, and mesh form.

References

Ali, M., Mansha, A., Asim, S., Zahid, M., Usman, M., & Ali, N. (2018). DFT Study for the Spectroscopic and Structural Analysis of p-Dimethylaminoazobenzene. *Journal of Spectroscopy, 2018*.

Ali, M., Subhani, M. S., Farhat Ibraheem, M. S., Hafeez, F., & Sana, K. A Computational Insight to Evaluate Performance of Fluorescein Dye, 7-Diethylamino-4-Methylcoumarin.

Ammar, Y. A., El-Hafez, S. M. A. A., Hessein, S. A., Ali, A. M., Askar, A. A., & Ragab, A. (2021). One-pot strategy for thiazole tethered 7-ethoxy quinoline hybrids: Synthesis and potential antimicrobial agents as dihydrofolate reductase (DHFR) inhibitors with molecular docking study. *Journal of molecular structure, 1242*, 130748. doi:https://doi.org/10.1016/j.molstruc.2021.130748

Ansbacher, T., Srivastava, H. K., Stein, T., Baer, R., Merkx, M., & Shurki, A. (2012). Calculation of transition dipole moment in fluorescent proteins—towards efficient energy transfer. *Physical Chemistry Chemical Physics, 14*(12), 4109-4117.

B, M., Bodke, Y. D., O, N., N, L. T., G, N., & Ma, S. (2021). Coumarin-Benzothiazole Based Azo Dyes: Synthesis, Characterization, Computational, Photophysical and Biological Studies. *Journal of molecular structure, 1246*, 131170. doi:https://doi.org/10.1016/j.molstruc.2021.131170

Baboul, A. G., Curtiss, L. A., Redfern, P. C., & Raghavachari, K. (1999). Gaussian-3 theory using density functional geometries and zero-point energies. *The Journal of chemical physics, 110*(16), 7650-7657.

Bagayoko, D. (2014). Understanding density functional theory (DFT) and completing it in practice. *AIP Advances, 4*(12).

Erdem Büyükkiraz, M., & Kesmen, Z. (2022). Antimicrobial peptides (AMPs): A promising class of antimicrobial compounds. *Journal of applied microbiology, 132*(3), 1573-1596.

Klähn, M., Mathias, G., Kötting, C., Nonella, M., Schlitter, J., Gerwert, K., & Tavan, P. (2004). IR spectra of phosphate ions in aqueous solution: predictions of a DFT/MM approach compared with observations. *The Journal of Physical Chemistry A, 108*(29), 6186-6194.

Mumit, M. A., Pal, T. K., Alam, M. A., Islam, M. A.-A.-A.-A., Paul, S., & Sheikh, M. C. (2020). DFT studies on vibrational and electronic spectra, HOMO–LUMO, MEP, HOMA, NBO and molecular docking analysis of benzyl-3-N-(2, 4, 5-trimethoxyphenylmethylene) hydrazinecarbodithioate. *Journal of molecular structure, 1220*, 128715.

Rani, A. U., Sundaraganesan, N., Kurt, M., Cinar, M., & Karabacak, M. (2010). FT-IR, FT-Raman, NMR spectra and DFT calculations on 4-chloro-N-methylaniline. *Spectrochimica Acta Part A: Molecular and Biomolecular Spectroscopy, 75*(5), 1523-1529.

Siddiqua, U. H., Irfan, M., Ali, S., Sahar, A., Khalid, M., Mahr, M. S., & Iqbal, J. (2020). Computational and experimental study of heterofunctional azo reactive dyes synthesized for cellulosic fabric. *Journal of molecular structure, 1221*, 128753. doi:https://doi.org/10.1016/j.molstruc.2020.128753

Zaman, Y., Ishaque, M. Z., Waris, K., Shahzad, M., Siddique, A. B., Arshad, M. I., . . . Mustaqeem, M. (2023). Modified physical properties of Ni doped ZnO NPs as potential photocatalyst and antibacterial agents. *Arabian Journal of Chemistry, 16*(11), 105230. doi:https://doi.org/10.1016/j.arabjc.2023.105230

Zhang, G., & Musgrave, C. B. (2007). Comparison of DFT methods for molecular orbital eigenvalue calculations. *The Journal of Physical Chemistry A, 111*(8), 1554-1561.

Authors:

First Author – Zunnaira Hakeem
Department of Chemistry, Riphah International University, Faisalabad, Pakistan
Second Author – Hina Masood,
Department of Chemistry, Government College University, Faisalabad, Pakistan
Third Author – Saba Nosheen,
Department of Chemistry, Riphah International University, Faisalabad.
Fourth Author– Muhammad Imran,
Department of Chemistry, Riphah International University, Faisalabad,
Fifth Author – Dr. Narmeen Ali, Department of Chemistry, Government College University, Faisalabad, Pakistan
Sixth Author – Laiba Waris,
Department of Chemistry, Riphah International University, Faisalabad
Seventh Author – Dr. Majid Ali,
Assistant Professor,
Department of Chemistry, Riphah International University, Faisalabad.
Eighth Author – Zahra Hanif,
Department of Chemistry, Riphah International University, Faisalabad.
Ninth Author: Dr. Sidra Ghafoor, Department of Chemistry, Government College University, Faisalabad, Pakistan
Tenth Author – Samiuddin, Researcher at
Department of Chemistry, Riphah International University, Faisalabad.
Correspondence Author – Dr. Majid Ali,
PHD Chemistry, Assistant professor,
Department of Chemistry, Riphah International University, Faisalabad.